RSC Advances

PAPER

View Article Online
View Journal | View Issue

Cite this: *RSC Adv.*, 2026, **16**, 19427

Synthesis and characterization of a new 2-iminothiolate-modified dimethacrylate monomer with potential dental applications

Rodrigo Pineda Mejía, *[abcd] Luis Fernando Giraldo Morales, [a] John Amalraj, [b] Rodrigo A. Giacaman *[c] and Leonardo Silva Santos *[d]

A 2-iminothiolate-functionalized dimethacrylate monomer (Bis-[GMA–TBA]) was rationally engineered to modulate network architecture and reduce polymerization shrinkage in methacrylate-based systems. The monomer was synthesized from bisphenol A-glycidyl methacrylate (Bis-GMA) through a sequential Mitsunobu azidation, Staudinger reduction, and post-functionalization with 2-iminothiolane. Structural integrity and successful side-chain incorporation were confirmed by FT-IR, ^{1}H NMR, and ESI-MS analyses. Photocurable matrices containing 50 wt% Bis-[GMA–TBA]/TEGDMA were formulated to evaluate structure-property relationships relative to conventional Bis-GMA/TEGDMA systems. The modified formulation exhibited a volumetric shrinkage of 8.2%, representing a ~27% reduction compared to the reference system (11.3%). Notably, this shrinkage reduction was achieved without compromising mechanical performance, as shear bond strength values remained comparable (55 ± 1.7 N *vs.* 49 ± 1.2 N), and marginal microleakage showed no significant differences. The reduced shrinkage is attributed to increased free volume and steric hindrance introduced by the bulky iminothiolate moiety, which modulates crosslink density and polymer network packing. These results demonstrate that targeted side-chain engineering provides an effective molecular strategy to tailor polymerization behavior while preserving mechanical integrity. This approach offers a versatile platform for the development of next-generation functional methacrylates for advanced biomedical materials.

Received 1st March 2026
Accepted 26th March 2026

DOI: 10.1039/d6ra01768a

rsc.li/rsc-advances

Introduction

Methacrylate-based composite resins are the dominant materials for direct dental restorations due to their aesthetic versatility, adhesive capability, and compatibility with minimally invasive procedures. However, polymerization shrinkage remains a fundamental limitation of dimethacrylate networks, compromising marginal integrity and promoting secondary caries formation.[1–5] The volumetric contraction that occurs during curing arises from the conversion of intermolecular van der Waals interactions into covalent bonds, resulting in increased crosslink density and reduced intermolecular distance.[1,3,6–8] This intrinsic physicochemical phenomenon continues to challenge the long-term stability of adhesive interfaces.[9–11]

Among commercial monomers, bisphenol A-glycidyl methacrylate (Bis-GMA) is widely used due to its rigidity and favorable mechanical properties. Nevertheless, its high viscosity and network packing contribute to significant polymerization shrinkage when copolymerized with low-molecular-weight diluents such as triethylene glycol dimethacrylate (TEGDMA).[1,8,12–14] Consequently, considerable research efforts have focused on modulating monomer structure to reduce shrinkage without sacrificing mechanical performance.[1,2,15–17] One rational strategy involves increasing molecular free volume through sterically demanding side-chain engineering, thereby reducing network densification during polymerization.[7,8,17,18]

Alternative approaches, including the incorporation of bioactive fillers and antimicrobial nanoparticles, have shown promising results in mitigating secondary caries.[19–23] However, these systems often rely on the release of active agents, which may compromise long-term stability due to leaching, porosity formation, or depletion of functional components.[14,22–26] These limitations highlight the need for molecular-level solutions that integrate functionality directly into the polymerizable monomer structure.[1,19,27,28]

In this context, we propose the rational design of a 2-iminothiolate-functionalized Bis-GMA derivative (Bis-[GMA–TBA]) as a strategy to simultaneously modulate network

[a]*Polymer Research Laboratory, Institute of Chemistry, University of Antioquia, Medellín, Colombia*

[b]*Laboratory of Materials Science, Institute of Chemistry of Natural Resources, University of Talca, 3460000, Talca, Chile. E-mail: ropm04@gmail.com*

[c]*Cariology Unit, Department of Oral Rehabilitation, Faculty of Dentistry, University of Talca, Talca, Chile. E-mail: giacaman@utalca.cl*

[d]*Laboratory of Asymmetric Synthesis, Institute of Chemistry of Natural Resources, Universidad de Talca, 3460000, Talca, Chile. E-mail: lssantos@utalca*

architecture and enhance functional performance. By introducing a bulky iminothiolate side group, we hypothesize an increase in internal free volume and altered crosslink packing, leading to reduced volumetric shrinkage without detrimental effects on mechanical integrity. This work explores the synthesis, structural characterization, and photopolymerization behavior of this novel monomer as a proof-of-concept for structure-property-guided development of advanced methacrylate networks for biomedical applications.

Experimental

Materials and reagents

All reagents were of analytical grade and used without further purification. Bis-GMA, methanol, dichloromethane (CH_2Cl_2), chloroform ($CHCl_3$), hexane, carbon tetrachloride (CCl_4), and *N*,*N*-dimethylformamide (DMF) were purchased from Merck KGaA (Darmstadt, Germany). Sodium hydroxide (NaOH), sulfuric acid (H_2SO_4), hydrochloric acid (HCl), sodium sulfate (Na_2SO_4), sodium borohydride ($NaBH_4$), disodium hydrogen phosphate (K_2HPO_4), sodium nitrate ($NaNO_3$), magnesium sulfate ($MgSO_4$), and ferrous sulfate ($FeSO_4$) were obtained from Thermo Scientific (Bedford, USA). Traut's reagent (2-iminothiolane) was purchased from Sigma-Aldrich (St. Louis, USA).

Instrumentation

All intermediates and final products were characterized using FT-IR and ESI-MS. The final product (Bis-[GMA–TBA]) was further confirmed by ^{1}H NMR (600 MHz). FT-IR analysis – samples (1.0 mg) were mixed with KBr (20 mg), pressed into pellets, and scanned using a Shimadzu IRAffinity-1 FT-IR spectrophotometer in the 4000–500 cm^{-1} range, with a resolution of 4 cm^{-1} (16 scans per sample). ^{1}H NMR analysis – Bis-[GMA–TBA] (5 mg) was dissolved in 0.5 mL of deuterated methanol and analyzed on a Bruker 600 MHz NMR spectrometer. Chemical shifts (δ) were reported in ppm and coupling constants (J) in Hz. ^{1}H NMR spectrum (600 MHz, CD_3OD) of Bis-[GMA–TBA]. A thiol proton is observed at δ 1.20 (t, 1H), along with methyl protons at δ 1.61 and 1.95 (s, 3H). Densities were determined using a Sartorius Quintix analytical balance with density kit YDK03.[29] Volumetric Shrinkage Assessment, volumes of the liquid (V_l) and solid (V_s) matrices were measured using glass capillaries (5 mm diameter × 20 mm length). Each formulation was analyzed in quadruplicate. Percentage of volumetric contraction (%ΔV), as reported in previous studies.[30–32] Specimen fabrication – specimens ($4 \times 4 \times 2$ mm^3) were prepared using Teflon molds. The matrix was cured with an LED lamp (400 mW cm^{-2}) for 40 s at a distance of 2 mm. The percentage of volumetric contraction was calculated as:

$$\%\,\Delta V = \frac{V_l - V_s}{V_l} \times 100\,\% \quad (1)$$

Contact angle analysis, static water contact angles (θ) were measured at 25 °C and 66% relative humidity. A 10 μL water droplet was placed using a Hamilton microsyringe, and images were acquired at 10–200× magnification. ImageJ software was used for analysis. Fifteen measurements per specimen were performed for both TBA50 and GMA50.[33] Thermogravimetric Analysis (TGA): TGA was performed on TBA50 and GMA50 samples (12.3–12.9 mg) using a TA Q500 analyzer under nitrogen (60 mL min^{-1}), in the range of temperature from 25 to 800 °C at the heating rate of 10 °C min^{-1}.[34] Scanning Electron Microscopy (SEM): SEM analysis was performed using a JEOL JSM-6490LV microscope under high vacuum. Samples were gold-coated using a Denton Vacuum Desk IV sputter coater and imaged with secondary electron detection to evaluate morphology.[35]

Methods

Synthesis of Bis-[GMA-N_3] (**1**) – Bis-GMA (1.0 mmol), sodium azide (NaN_3, 2.4 mmol), and triphenylphosphine (PPh_3, 4.2 mmol) were dissolved in 10 mL of anhydrous CCl_4/DMF (1 : 4 v/v) under constant stirring. The reaction mixture was refluxed for 24 h and monitored by thin-layer chromatography (TLC) and Fourier transform infrared spectroscopy (FT-IR). Upon completion, the mixture was cooled to room temperature, quenched with 5 mL of double-distilled water, and stirred for 30 min. The organic phase was separated, washed with water (3 × 5 mL), dried over anhydrous Na_2SO_4, and purified as described in section purification.

Synthesis of Bis-[GMA-NH_2] (**2**) – Bis-[GMA-N_3] (1.0 mmol) and PPh_3 (2.4 mmol) were dissolved in 10 mL of anhydrous CCl_4/DMF (1 : 4 v/v) and refluxed for 24 h under constant stirring. The reaction was monitored by TLC. After cooling, 5 mL of double-distilled water was added, and the mixture was stirred for an additional 24 h. The organic layer was washed with water (3 × 5 mL), dried with Na_2SO_4, and purified as described in section Purification.

Synthesis of Bis-[GMA–TBA] (**3**) – Bis-[GMA-NH_2] (1.0 mmol) and 2-iminothiolane (2.4 mmol) were stirred in methanol (10 mL) at 40 °C for 12 h. The solvent was evaporated under reduced pressure, and the residue was extracted with CH_2Cl_2/H_2O (1 : 1 v/v). The organic phase was dried over Na_2SO_4.

Experimental conditions

All compounds were purified by column chromatography. Thin-layer chromatography (TLC) was performed on silica gel 60 F254 plates (0.25 mm thickness), using a mobile phase of CH_2Cl_2/$CHCl_3$/MeOH (6 : 2 : 2 v/v). Visualization was done under UV light (254/365 nm) and with a universal reagent (acetic acid/H_2SO_4/H_2O, 71 : 14 : 15), followed by mild heating. For preparative chromatography, silica gel 60 (0.040–0.063 mm) was used, with polarity gradient elution using $CHCl_3$/MeOH. Final purification employed Sephadex LH-20 and hexane/CH_2Cl_2/MeOH (50 : 25 : 25).[36]

Data collection and analysis

Data normality was tested using the Kolmogorov–Smirnov test. ANOVA followed by Tukey's test was applied for normally distributed data; otherwise, the Kruskal–Wallis test was used.

Table 1 Composition of acrylic matrices (wt%)

Component\matrix	TBA50	GMA50	TEG99
Bis-[GMA–TBA]	49.5	0	0
Bis-GMA	0	49.5	0
TEGDMA	49.5	49.5	99
Camphorquinone	0.5	0.5	0.5
4 *N*,*N*-Trimethylaniline	0.5	0.5	0.5

Differences were considered statistically significant at $p < 0.05$. All analyses were performed using R software, and the coefficient of variation was calculated as the standard deviation relative to the mean.

Extra information

2,2-Bis[4-(2′-hydroxy-3′-methacryloyloxypropoxy)phenyl] propane, its commercial name Bis-GMA.

IR (KBr, cm^{-1}) 3458, 1720, 1635, 1600 y 1500, 1250–1100; ESI-MS *m*/*z*, calcd. for $[C_{29}H_{36}O_8 + \mathbf{Na}]^+$: 535.6, found: 535.3.

2,2-Bis[4-(2′-azide-3′-methacryloyloxypropoxy)phenyl] propane (**1**) new compound and will be called Bis-[GMA-N_3].

IR (KBr, cm^{-1}) 2104, 1720, 1635, 1600 y 1500, 1250–1100; ESI-MS *m*/*z*, calcd. for $[C_{29}H_{34}N_6O_6 + \mathbf{H}]^+$: 563.6, found: 562.6.

2,2-Bis[4-(2′-amine-3′-methacryloyloxypropoxy)phenyl] propane (**2**) new compound and will be called Bis-[GMA-NH_2].

IR (KBr, cm^{-1}) 3284, 1720, 1635, 1600 y 1500, 1250–1100; ESI-MS *m*/*z*, calcd. for $[C_{29}H_{38}N_2O_6 + \mathbf{Na}]^+$: 533.6, found: 533.3.

2,2-Bis[4-(2′-thio-butylamidine-3′-methacryloyloxypropoxy) phenyl]propane (**3**) new compound and will be called Bis-[GMA–TBA].

IR (KBr, cm^{-1}) 3339, 1720, 1635, 1600 y 1500, 1250–1100; ESI-MS *m*/*z*, calcd. for $[C_{37}H_{54}Cl_2N_4O_6S_2 + H]$: 786,9, found: 785.9. ^{1}H NMR (600 MHz, CD_3OD) δ (ppm) 1.20 (t, 1H, *J* 7, SH), 1.61 (s, 1H, =C–H), 1.95 (s, 3H, –C–CH_3), 2.40 (m, 2H, C–CH_2–C), 3.40 (m, 2H, –CH_2–S–), 3.63 (t, 2H, =C–CH_2–CH_2–), 4.03 (d, 2H, *J* 7, –O–CH_2–CH–), 4.20 (d, 2H, *J* 7, CH–CH_2–O–), 4.35. (m, 1H, CH_2–CH–CH_2–), 4.91 (br s, 2H, NH_2^+), 5.65 (S, 1Ha, =C–Ha), 6.15 (s, 1Hb, =C–Hb), 6.84 (d, 2H, $J = 7.9$ Hz), 7.12 (d, 2H, $J = 8.8$ Hz).

Preparation of photopolymerizable resin formulations

The experimental resin formulations were prepared using Bis-[GMA–TBA] or Bis-GMA as the base dimethacrylate monomer. Each monomer was blended with 49.5 wt% triethylene glycol dimethacrylate (TEGDMA) as a reactive diluent, together with 0.5 wt% camphorquinone and 0.5 wt% 4-(*N*,*N*-dimethylamino) aniline as the photoinitiator system. The mixtures were stored in amber vials at 5 °C until use.

For clarity, the formulations were coded according to the base dimethacrylate monomer present at approximately 50 wt% in the resin matrix: TBA50 (Bis-[GMA–TBA]/TEGDMA) and GMA50 (Bis-GMA/TEGDMA). The GMA50 formulation served as the reference system, while a formulation containing 99 wt% TEGDMA with the same photoinitiator system was used as an additional control (TEG99). The codes assigned to each formulation are summarized in Table 1.

The potential oxidation of sulfhydryl groups to disulfides was not specifically investigated in this study. However, the resin formulations were stored in amber vials at 5 °C and used within a short period after preparation, conditions that minimize oxidative processes. In addition, the thiol functionality is incorporated within a sterically demanding iminothiolane-derived side group, which may reduce intermolecular thiol–thiol interactions prior to photopolymerization.

Results

Characterization of Bis-[GMA-N_3] (1) by FT-IR and ESI-MS

The precursor monomer Bis-GMA was initially characterized by FT-IR spectroscopy to confirm the presence of its characteristic functional groups. A broad absorption band centered at 3458 cm^{-1} was assigned to the O–H stretching vibration.

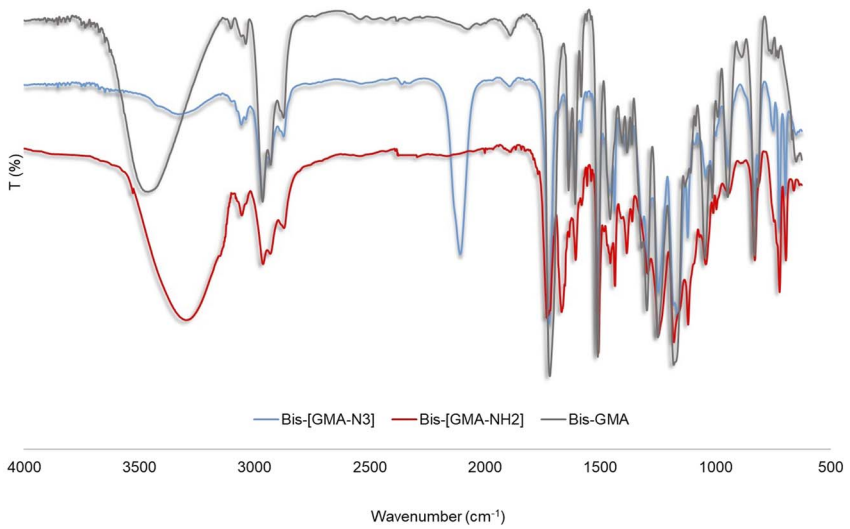

Fig. 1 FT-IR spectra for Bis-GMA, Bis-[GMA-N_3], (**1**), and Bis-[GMA-NH_2], (**2**).

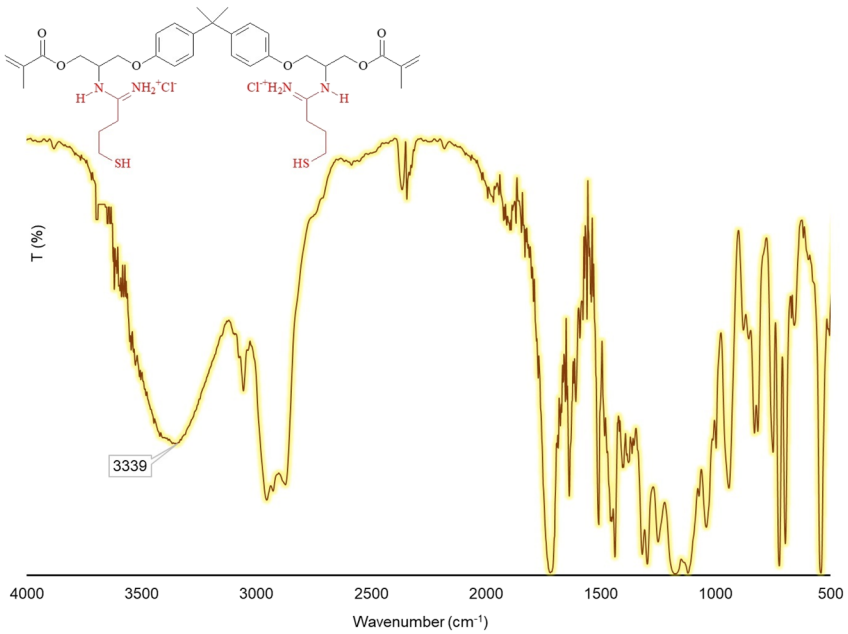

Fig. 2 FT-IR spectrum of Bis-[GMA–TBA], obtained after the reaction between Bis-[GMA-NH_2] and 2-iminothiolane. The disappearance of the amine band at 3284 cm^{-1} and the appearance of the characteristic amidine band at 3339 cm^{-1} are observed.

Additional diagnostic signals included the ester carbonyl stretching at 1718 cm^{-1} and aliphatic C–H stretching vibrations in the 2800–3000 cm^{-1} region (Fig. 1).

The ESI-MS spectrum displayed a molecular ion peak at *m*/*z* 535.3, corresponding to the sodium adduct $[M + Na]^+$ of $C_{29}H_{36}O_8$ (calcd *m*/*z* 512.59), confirming the expected molecular mass (Fig. S6).

Following nucleophilic substitution of the hydroxyl groups with azide functionalities *via* a modified Mitsunobu reaction (Fig. 2, Reaction 1). Bis-[GMA-N_3] (1) was obtained in 63% yield. The FT-IR spectrum of compound (**1**) showed complete disappearance of the O–H stretching band and the emergence of a new sharp absorption at 2104 cm^{-1}, characteristic of the asymmetric stretching vibration of the azide group, confirming successful functionalization (Fig. 1). The ESI-MS spectrum of (1) exhibited a molecular ion peak consistent with the protonated species $[M + H]^+$ of $C_{29}H_{34}N_6O_6$ (calcd *m*/*z* 562.60) (Fig. S7), further supporting the proposed structure.

Characterization of Bis-[GMA-NH_2] by FT-IR and ESI-MS. Bis-[GMA-NH_2], (**2**), was synthesized *via* Staudinger reduction of the azide group in Bis-[GMA-N_3] (Scheme 1, Reaction 2). The FT-IR spectrum confirmed the conversion by showing the disappearance of the azide band at 2104 cm^{-1} and the appearance of a broad band at 3284 cm^{-1}, corresponding to N–H stretching of the primary amine (Fig. 1). Other characteristic signals remained unchanged. The isolated yield was 44%. ESI-MS revealed a peak at *m*/*z* 533.3, attributed to $[M + Na]^+$ (calcd *m*/*z* 532,98) (Fig. S8).

Characterization of Bis-[GMA–TBA] by FT-IR, ESI-MS, and ^{1}H NMR. Bis-[GMA–TBA] was obtained through the reaction of Bis-[GMA-NH_2] with 2-iminothiolane (Traut's reagent) (Scheme 1, Reaction 3). The product contains an amidine moiety [–C(=NH)–NH–], which is analogous to an amide but with an imino group replacing the carbonyl oxygen. FT-IR analysis showed the disappearance of the amine band (3284 cm^{-1}) and the appearance of a broad signal at 3339 cm^{-1}, indicative of the newly formed amidine group (Fig. 2). The isolated yield was 11%. The ESI-MS spectrum of the compound with molecular formula $C_{37}H_{54}Cl_2N_4O_6S_2$ exhibited two prominent peaks at *m*/*z* 785.9 and 808.9, corresponding to the $[M + H]^+$ and $[M + Na]^+$ ions, respectively. These signals are in excellent agreement with the calculated monoisotopic mass of the neutral molecule (calcd *m*/*z* 784.3), confirming the molecular identity (Fig. S9).

The ^{1}H NMR spectrum of Bis-[GMA–TBA] (CD_3OD, 600 MHz) showed the following signals (Fig. S10): a thiol proton at δ 1.20 (t, 1H), methyl protons at δ 1.61 and 1.95 (s, 3H), methylene protons from the thio-butylamidine group at δ 2.40 (m, 2H), 3.40 (m, 2H), and 3.63 (t, 2H), and olefinic and benzylic protons between δ 4.03 and 4.35. The amidine group appeared as a broad signal at δ 4.91. Vinyl protons resonated at δ 5.65 and 6.15 (s, 1H), while aromatic protons appeared at δ 6.84 (d, 2H, J = 7.9 Hz) and δ 7.12 (d, 2H, J = 8.8 Hz).

Volumetric contraction of TBA50, GMA50, and TEG99. The volumes of the monomeric formulations TBA50, GMA50, and TEG99 in both liquid and polymerized (solid) states are shown in Table 2. The percentage of volumetric contraction (%ΔV) was calculated according to eqn (1), and the results are summarized in Fig. 3. The highest coefficient of variation observed among the measurements was 8.5%.

The measured volumetric contraction for TEG99 was 13.7%, which closely aligns with previously reported values, indicating the reliability of the methodology. Literature data also indicate a contraction of 6.1% for pure Bis-GMA. Based on this, a 50 : 50 Bis-GMA : TEGDMA mixture (GMA50) was expected to show

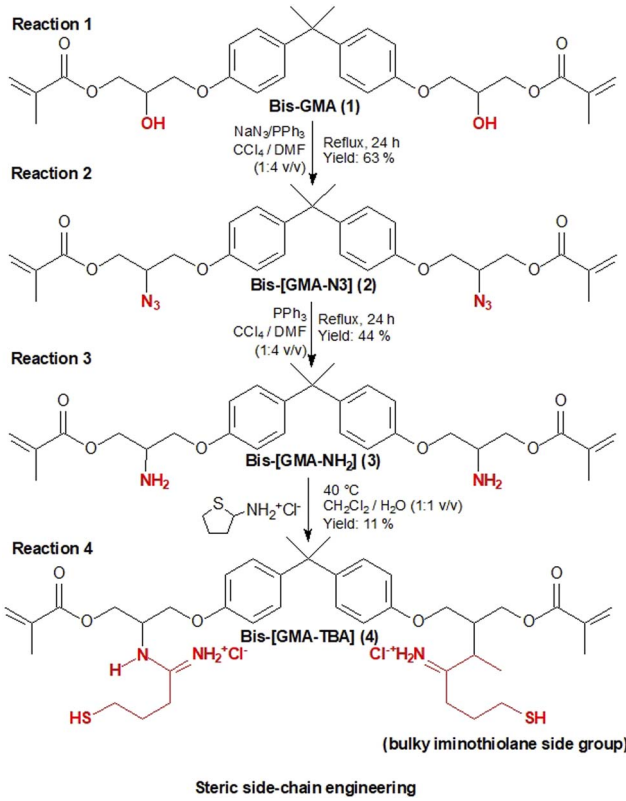

Scheme 1 Molecular design and synthesis. Reaction 1: Bis-GMA is treated with sodium azide (NaN_3) and triphenylphosphine (PPh_3), previously dissolved in DMF, to perform the nucleophilic substitution of the hydroxyl groups by azide groups at reflux temperature for 24 h. Reaction 2: the compound obtained in Reaction 1 (Bis-[GMA-N_3]) is treated with PPh_3 to reduce the azide groups to amine groups, also at reflux temperature for 24 h. Reaction 3: finally, the compound from Reaction 2 (Bis-[GMA-NH_2]) is reacted with 2-iminothiolane at 40 °C for 12 h to obtain Bis-[GMA–TBA].

Table 2 Volumes of the monomeric (liquid) and polymerized (solid) matrices

Matrix	Liquid matrix (mm^3)	Solid matrix (mm^3)
TBA50	113.4 ± 8.7	103.7 ± 7.0
GMA50	132.3 ± 15.5	117.4 ± 13.9
TEG99	115.2 ± 14.0	99.4 ± 11.9

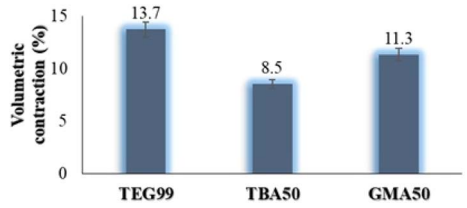

Fig. 3 Volumetric contraction of the experimental monomer systems. Statistical analysis revealed significant differences among the groups (ANOVA, $p = 0.0002$).

intermediate contraction, which was confirmed by the measured value of 11.3%.

Volumetric shrinkage occurs due to the reduction in intermolecular distances when a monomer transforms into a polymer. This is governed by the free volume between molecules, which varies depending on the substituents in the polymer chain. For example, TEG99, lacking bulky substituents, exhibited the highest shrinkage. Conversely, TBA50 showed the lowest shrinkage (8.5%), suggesting a greater free volume, likely due to the bulkiness of the Bis-[GMA–TBA] moiety. The molar masses of the monomers (Table S4) further support these observations. TEGDMA (286.3 g mol^{-1}) has a lower molar mass than Bis-GMA (512.6 g mol^{-1}), correlating with higher volumetric contraction. Notably, TBA50, composed of 50 wt% Bis-[GMA–TBA] and 50 wt% TEGDMA, exhibited lower shrinkage than GMA50, despite both having the same TEGDMA content. This difference may be attributed to the higher molar mass of Bis-[GMA–TBA] (785.9 g mol^{-1}), which is approximately 1.5 times greater than that of Bis-GMA, resulting in fewer reactive sites and lower overall contraction.

Density of TBA50 and GMA50 resin formulations and corresponding polymers. The densities of the polymerized TBA50 and GMA50 matrices, determined using an analytical balance, were 1233.8 and 1237.9 kg m^{-3}, respectively. The densities of the corresponding uncured resin formulations were 1128.3 kg m^{-3} for TBA50 and 1098.1 kg m^{-3} for GMA50.

Both formulations consist of 50 wt% triethylene glycol dimethacrylate (TEGDMA) and 50 wt% of the base dimethacrylate monomer, corresponding to Bis-[GMA–TBA] in TBA50 and Bis-GMA in GMA50. Reported density values for TEGDMA in the liquid and polymerized states have been previously described in the literature.

These density values were used in the calculation of volumetric shrinkage during polymerization.

Table 3 summarizes the density values of the uncured resin formulations and the corresponding polymer networks.

Contact angle of TBA50 and GMA50. The water contact angles measured for the TBA50 and GMA50 resins were 60.0° ± 0.5° and 63.0° ± 0.2°, respectively ($p < 0.001$; Fig. 4). The lower contact angle observed for TBA50 indicates improved surface wettability, which may be advantageous for dental photorestorative applications.

Thermal stability (TGA) of poly(GMA50) and poly(TBA50). Thermogravimetric analysis (TGA) of poly(GMA50) revealed a three-step degradation profile. The first mass loss occurred between 25 and 243 °C, followed by additional decomposition

Table 3 Density of uncured resins and corresponding polymer networks[a]

Matrix	Density of uncured resin (kg m^{-3})	Density of polymer (kg m^{-3})
GMA50	1128.3	1233.8
TBA50	1098.06	1237.9

[a] GMA50: 50 wt% Bis-GMA/50 wt% TEGDMA; TBA50: 50 wt% Bis-[GMA–TBA]/50 wt% TEGDMA.

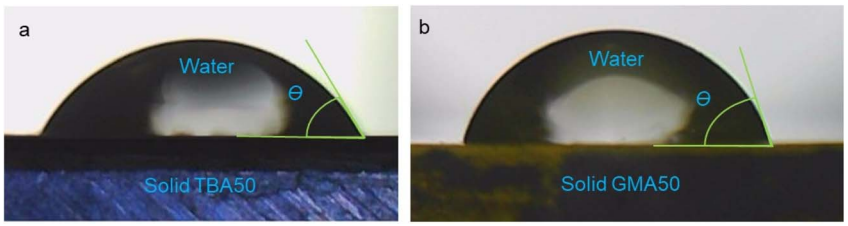

Fig. 4 Water contact angle measurements for (a) TBA50 and (b) GMA50.

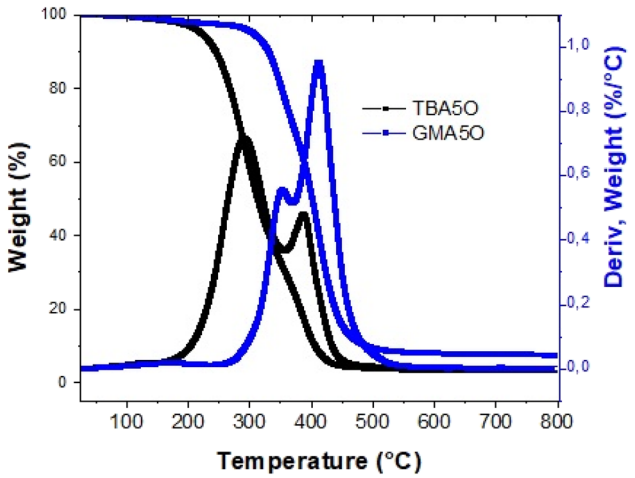

Fig. 5 TGA curves of poly(GMA50) and poly(TBA50) recorded under nitrogen atmosphere at a heating rate of 10 °C min^{-1} from 25 to 600 °C. SEM analysis of poly(GMA50) and poly(TBA50).

steps up to 625 °C. These results are consistent with previously reported data. Poly(TBA50) also exhibited a three-step degradation process, with mass losses occurring between 25–140 °C, 140–357 °C, and 357–520 °C, leaving a final residue of 3.3% (Fig. 5).

The surface morphology of the polymers was examined by scanning electron microscopy (SEM) at different magnifications. Images (a) and (b), corresponding to poly(GMA50), revealed a smooth, compact fracture surface with no evidence of particulate debris, cracks, or delamination. The fracture edges appear continuous and cohesive, suggesting a homogeneous internal structure and good mechanical integrity. These characteristics indicate that the polymer matrix is well-formed and resistant to brittle failure under the conditions applied. In contrast, images (c) and (d), assigned to poly(TBA50), exhibited clear signs of fracture propagation accompanied by the formation of irregular fragments and debris. At higher magnification (d), rough fracture zones and radial crack patterns can be observed, which are typical of brittle materials undergoing stress concentration and failure. The presence of microcracks and broken domains may reflect differences in chain packing, stiffness, or phase segregation induced by the monomeric composition. Overall, SEM analysis reveals that the TBA-based polymer has a more heterogeneous and fragile structure compared to the GMA-based counterpart (Fig. 6).

Discussion

The Mitsunobu reaction typically employs PPh_3 and diethyl azodicarboxylate (DEAD); however, in this study, DEAD was replaced by NaN_3, enabling the nucleophilic substitution of the two hydroxyl groups in Bis-GMA with two azide groups, yielding Bis-[GMA-N_3]. Similar substitutions have been reported using different substrates.[37] The subsequent Staudinger reduction of Bis-[GMA-N_3] afforded Bis-[GMA-NH_2] in good yield. This reaction proceeds *via* the formation of an aza-ylide intermediate, which hydrolyzes spontaneously to give the corresponding primary amine and phosphine oxide.

Further modification of the molecule was achieved by reacting Bis-[GMA-NH_2] with 2-iminothiolane (Traut's reagent), which is known for its specificity toward primary amines. This reaction introduced a spacer arm of 8.2 Å terminating in a thiol group, resulting in the formation of Bis-[GMA–TBA]. This type of derivatization has been previously applied in chitosan-TBA conjugates, where a high density of thiol groups was achieved. Successful reactions of Traut's reagent with protein amines with good yields and selectivity have also been documented. The novel photopolymerizable monomer Bis-[GMA–TBA] synthesized in this work features an extended lateral arm and a 53% increase in molar mass compared to Bis-GMA. These structural modifications are expected to influence the polymer network architecture and reduce volumetric shrinkage, making the compound a promising candidate for advanced dental restorative applications (Fig. 7).

Under the employed photopolymerization conditions, chain-growth polymerization of methacrylate double bonds is kinetically favored over potential thiol-mediated reactions. Therefore, the network formation is expected to be governed primarily by the dimethacrylate functionality of the monomer.[11,38]

During polymerization, monomeric units transition from weak van der Waals interactions (with intermolecular distances of approximately 3.4 Å) to covalent carbon–carbon bonds of about 1.54 Å, leading to volumetric shrinkage.[13,39] Linear polymers typically exhibit greater shrinkage than branched polymers due to their ability to pack more efficiently into ordered lamellar structures.[11] In contrast, bulky or branched side groups introduce steric hindrance, limiting chain packing efficiency and increasing the free volume between polymer chains, thereby reducing overall contraction.[40] This structural effect explains the observed difference in volumetric shrinkage between the control matrix GMA50 (11.3%) and the experimental matrix TBA50 (8.5%), with the former showing

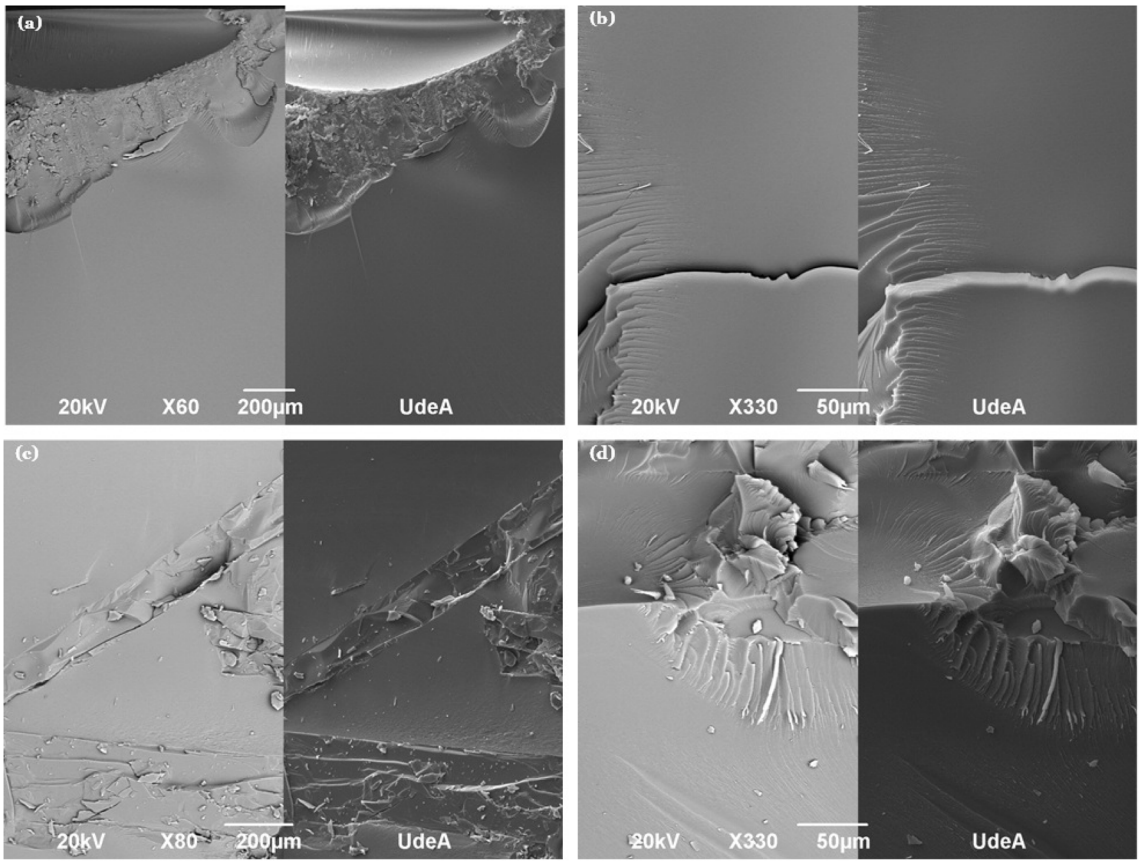

Fig. 6 Scanning electron microscopy (SEM) images of poly(GMA50) and poly(TBA50) fractured surfaces. Images (a) and (b) correspond to poly(GMA50) at magnifications of 200 μm and 50 μm, respectively, showing a smooth and homogeneous surface without evidence of debris upon fracture. Images (c) and (d) correspond to poly(TBA50) at the same magnifications, revealing irregular fracture patterns and the presence of particulate matter resulting from mechanical failure.

approximately 1.3 times higher shrinkage. Microleakage, defined as the ingress of bacteria, fluids, molecules, and ions between the restorative material and the tooth interface, is a primary contributor to the development of secondary caries and remains a critical challenge in the long-term success of dental restorations.[3,41] This failure is often associated with polymerization-induced volumetric contraction and inadequate adaptation of the restorative material to the cavity walls, which can create interfacial gaps and promote microleakage.[3,42–44] Among the tested polymers, poly(TEGDMA) exhibited the highest volumetric contraction, likely due to its low free volume and highly flexible molecular structure, which facilitates dense packing of polymer chains during polymerization. In contrast, the rigid bisphenol A backbone in Bis-GMA imparts significant molecular stiffness, which limits segmental mobility during polymerization. This reduced flexibility slows the degree of conversion and leads to a more heterogeneous and less organized polymer network.[1,8,45]

The newly synthesized monomer Bis-[GMA–TBA] retains the molecular rigidity of the bisphenol A core of Bis-GMA, while incorporating a bulky thiobutylamidine side group. This substitution increases the free volume (~8.2 Å) compared to both TEGDMA and Bis-GMA, thereby reducing the volumetric contraction observed during polymerization. The estimated density of poly(Bis-[GMA–TBA]) was found to be lower than that of poly(Bis-GMA) and poly(TEGDMA), which is consistent with the incorporation of bulky, branched thiobutylamidine side groups. These groups hinder the tight packing of the polymer chains, thereby increasing the specific volume of the polymer. Reported values for poly(Bis-GMA) and poly(TEGDMA) are 1226 and 1250 kg m^{-3}, respectively, which closely match our calculated densities for Bis-GMA and Bis-[GMA–TBA].[46–49] These results validate the accuracy of the indirect estimation method employed, which was necessary due to the high viscosity and handling difficulty of Bis-[GMA–TBA]. The observed differences in contact angles between TBA50 and GMA50 can be explained by their distinct surface chemistries. The amidine moiety (–C(=NH)–NH–) in Bis-[GMA–TBA] enhances hydrophilicity through both hydrogen bonding and ion-dipole interactions with water molecules. Such behavior is consistent with the known capacity of amidines to engage in robust hydrogen bonding due to their protic nature and delocalized charge. Consequently, surfaces bearing amidine functionalities tend to exhibit lower water contact angles and improved wettability. Additionally, the thiol (–SH) functional groups present in TBA50 contribute to enhanced wettability by enabling dipole–dipole interactions

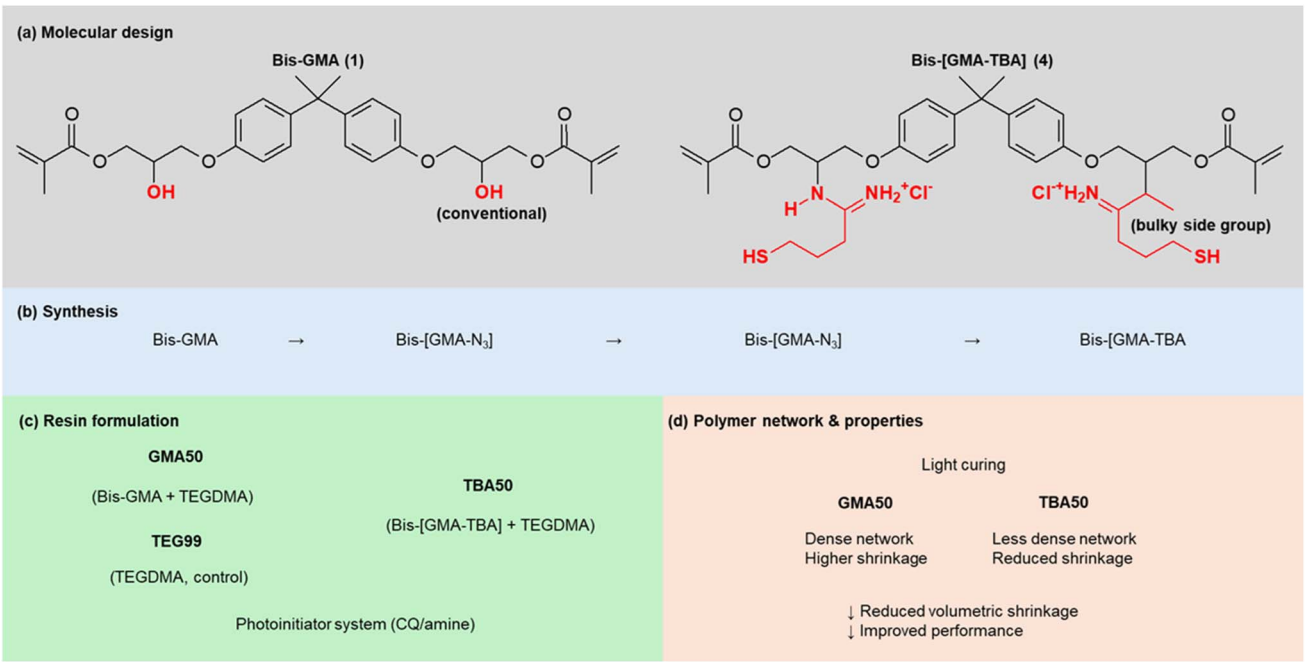

Fig. 7 Schematic overview of the molecular design, synthesis, resin formulation, and resulting polymer network properties of Bis-[GMA-TBA]-based systems. (a) Molecular design of Bis-GMA and the modified Bis-[GMA-TBA] monomer, highlighting the introduction of a bulky iminothiolane-derived side group. (b) Synthetic route from Bis-GMA to Bis-[GMA-TBA] *via* azidation and subsequent reduction steps. (c) Resin formulations, including GMA50 (Bis-GMA/TEGDMA), TBA50 (Bis-[GMA-TBA]/TEGDMA), and TEG99 (TEGDMA control), using a CQ/amine photoinitiator system. (d) Schematic representation of the polymer networks after light curing, comparing GMA50 (dense network, higher shrinkage) and TBA50 (less dense network, reduced shrinkage), leading to improved performance.

with water molecules. Sulfhydryl-terminated polymers have been shown to exhibit lower contact angles and increased hydrophilicity compared to their non-thiol counterparts. In contrast, GMA50 contains hydroxyl (–OH) groups capable of forming strong hydrogen bonds with water, enhancing hydrophilicity, albeit to a lesser extent than amidine and thiol interactions, thus explaining the observed differences in contact angle.

Consequently, TBA50 exhibited a significantly lower contact angle than GMA50, indicating superior wettability. Reported water contact angle values for dentin typically range between 60° and 70°, while commercial resin-based composites generally exhibit values between 65° and 85°, depending on their composition and surface characteristics. In dental restorative applications, lower contact angles are generally associated with improved wettability and enhanced interfacial interaction with the tooth substrate.[2,11,50,51] Therefore, the contact angle observed for TBA50 suggests enhanced adhesion potential to dental tissues and promising clinical performance compared to conventional Bis-GMA-based systems. Further studies exploring the effect of monomer concentration on the physicochemical properties of these systems are currently underway and will be reported in future work. The comparison between GMA50 and TBA50 enables the evaluation of the combined effect of amidine and thiol functionalities introduced through the molecular modification.

Overall, the results highlight the potential of molecular engineering strategies to tailor the architecture of dimethacrylate monomers for improved performance in dental resin systems. By introducing a sterically demanding thiobutylamidine side group into the Bis-GMA framework, the newly synthesized Bis-[GMA–TBA] monomer modifies intermolecular packing within the polymer network, leading to reduced volumetric shrinkage while preserving favorable physicochemical properties. This structure-property relationship suggests that controlled incorporation of bulky functional groups into conventional dental monomers may represent a promising approach for the development of next-generation restorative materials with improved dimensional stability and interfacial performance.

Conclusions

A novel photopolymerizable monomer, Bis-[GMA–TBA], was successfully synthesized and structurally confirmed by FT-IR, ESI-MS, and ^{1}H NMR spectroscopy. Incorporation of a bulky thiobutylamidine moiety led to reduced volumetric shrinkage (8.5%) and lower calculated polymer density compared to conventional Bis-GMA-based systems. These effects are attributed to the increased molar mass and enhanced free volume, which disrupt efficient chain packing and limit contraction during curing.

The modified structure also resulted in improved surface wettability, suggesting favorable interfacial characteristics. The synthetic strategy presented herein demonstrates a modular

approach for the rational design of functional monomers with tailored physicochemical properties.

Overall, this study provides structural and physicochemical evidence supporting Bis-[GMA–TBA] as a promising candidate for the development of low-shrinkage photopolymer networks. Further investigations into polymerization kinetics, mechanical performance, and long-term biocompatibility are warranted to fully assess its applicability in dental and biomedical materials.

Ethical statement

The study does not require approval from an ethics committee.

Author contributions

RP: conception, design, data acquisition, data analysis and drafting of the first manuscript. LSS, LG and JA: data analysis and critical revision of the manuscript. RAG: conception, data analysis, editing of the manuscript and critical revision of the manuscript. All authors gave their final approval and agreed to be accountable for all aspects of the work.

Conflicts of interest

The authors declare no conflicts of interest.

Data availability

The data supporting this study are available within the article and its supplementary information (SI). Additional data are available from the corresponding author upon reasonable request. Supplementary information: experimental data and characterization results supporting the findings of this study. Fig. S1 and S2 present the methodology used for capillary diameter measurements, including optical and microscopic analysis. Fig. S3–S5 show FT-IR spectra confirming the chemical modification of Bis-GMA, including functional group transformations. Fig. S6–S9 display ESI-MS spectra validating the molecular structures of the synthesized compounds. Fig. S10 presents the ^{1}H NMR spectrum of Bis-[GMA-TBA], confirming its chemical structure. Fig. S11 shows SEM images comparing the macroscopic and microstructural morphology of the GMA50 and TBA50 polymers. Fig. S12–S14 illustrate schematic representations of polymerization processes and their relationship with volumetric contraction behavior. SI Tables S1–S4 include estimated polymer densities, thermogravimetric analysis (TGA) data, and theoretical molar masses of the studied compounds. Additionally, eqn S1–S8 detail the calculations used to determine capillary dimensions, resin volumes, volumetric contraction, and density estimations. These supplementary data provide comprehensive support for the structural characterization, physicochemical analysis, and polymerization behavior discussed in the main manuscript. See DOI: https://doi.org/10.1039/d6ra01768a.

Acknowledgements

Funding for this study was partially provided by the Chilean Government agency ANID, Grant Fondecyt 1210188 to RAG. The study also received support from a scholarship from the University of Talca and the LIPOL research group at the University of Antioquia. The funders had no role in the study, design, data collection and analysis, decision to publish, or preparation of the manuscript.

References

1 N. B. Cramer, J. W. Stansbury and C. N. Bowman, *J. Dent. Res.*, 2011, **90**, 402–416.
2 N. Ilie, *Aust. Dent. J.*, 2011, **56**, 59–66.
3 R. R. Braga, R. Y. Ballester and J. L. Ferracane, *Dent. Mater.*, 2005, **21**, 962–970.
4 S. Ivanova, Z. Tomova, A. Vlahova, I. L. Stoeva, E. Vasileva, Y. Uzunova, M. Urumova, D. Tomov and A. Chonin, *Polymers*, 2026, **18**, 138.
5 D. Weimann, C. Fleck and H. Razi, *J. Mech. Behav. Biomed. Mater.*, 2024, **155**, 106554.
6 J. W. Stansbury and M. J. Idacavage, *Dent. Mater.*, 2016, **32**, 54–64.
7 C. Pfeifer, N. Wilson and Z. Shelton, *Polymer*, 2011, **52**, 3295–3303.
8 J. Elliott and L. Lovell, *Dent. Mater.*, 2001, **17**, 221–229.
9 P. Spencer, Q. Ye, A. Misra, S. E. P. Goncalves and J. S. Laurence, *J. Dent. Res.*, 2014, **93**, 1243–1249.
10 J. De Munck, K. Van Landuyt, M. Peumans, A. Poitevin, P. Lambrechts, M. Braem and B. Van Meerbeek, *J. Dent. Res.*, 2005, **84**, 118–132.
11 J. L. Ferracane, *Dent. Mater.*, 2011, **27**, 29–38.
12 R. L. Bowen, *J. Am. Dent. Assoc.*, 1963, **66**, 57–64.
13 I. Sideridou and V. Tserki, *Biomaterials*, 2003, **24**, 655–665.
14 I. Sideridou, *J. Biomed. Mater. Res. B Appl. Biomater.*, 2005, **74**, 617–626.
15 W. Weinmann and C. Thalacker, *Dent. Mater.*, 2005, **21**, 68–74.
16 C. Pfeifer, *Sci. World*, 2019, **11**, 295–333.
17 A. Bacchi and C. S. Pfeifer, *Materials*, 2016, **32**, 978–986.
18 C. N. Bowman and C. J. Kloxin, *AIChE J.*, 2008, **54**, 2775–2795.
19 M. A. S. Melo, L. Cheng, M. D. Weir, R. C. Hsia, L. K. A. Rodrigues and H. H. K. Xu, *J. Biomed. Mater. Res. B Appl. Biomater.*, 2013, **101**, 620–629.
20 P. Zhang, G. Zhang and X. Shang, *Forests*, 2022, **13**, 1626.
21 S. Imazato, *Dent. Mater.*, 2023, **19**, 449–457.
22 A. Besinis, T. De Peralta and R. D. Handy, *Nanotoxicolog*, 2014, **8**, 1–16.
23 L. Cheng, M. Weir, H. Xu and J. A.-D. Materials, *Dent. Mater.*, 2012, **28**, 561–572.
24 K. Van Landuyt, T. Nawrot and B. Geebelen, *Dent. Mater.*, 2011, **27**, 723–747.
25 D. Khvostenko, J. Mitchell, T. Hilton and J. L. Ferracane, *Dent. Mater.*, 2013, **29**, 1139–1148.

26 M. Cadenaro, T. Maravic, A. Comba, A. Mazzoni, L. Fanfoni, T. Hilton, J. Ferracane and L. Breschi, *Dent. Mater.*, 2019, **35**, e1–e22.
27 K. Zhang, L. Cheng, M. D. Weir, Y. X. Bai and H. H. K. Xu, *Int. J. Oral Sci.*, 2015, **8**(1), 45–53.
28 S. Imazato, S. Ma and J. Chen, *Dent. Mater.*, 2014, **30**, 97–104.
29 N. J. Walters, W. Xia, V. Salih, P. F. Ashley and A. M. Young, *Dent. Mater.*, 2016, **32**, 264–277.
30 M. Topa-Skwarczyńska and J. Ortyl, *Polym. Chem.*, 2023, **14**, 2145–2158.
31 A. Szczesio-Wlodarczyk, S. Garoushi, P. Vallittu, K. Bociong and L. Lassila, *Dent. Mater. J.*, 2024, **43**, 155–163.
32 M. Gallo, H. Abouelleil, J. M. Chenal, J. Adrien, J. Lachambre, P. Colon and E. Maire, *Dent. Mater.*, 2019, **35**, 1654–1664.
33 F. M. Namen, E. Ferrandini and J. Galan Junior, *J. Appl. Oral Sci.*, 2011, **19**, 517–520.
34 R. R. Braga and J. L. Ferracane, *Crit. Rev. Oral Biol. Med.*, 2004, **15**, 176–184.
35 M. A. Melo, S. Orrego, M. D. Weir, H. H. K. Xu and D. D. Arola, *ACS Appl. Mater. Interfaces*, 2016, **8**, 11779–11787.
36 R. Pineda, S. Vizcaíno, C. M. García, J. H. Gil and D. Durango, *Rev. Fac. Nac. Agron. Medellin*, 2018, **71**, 8563–8572.
37 A. Saito, K. Saito, A. Tanaka and T. Oritani, *Tetrahedron Lett.*, 1997, **38**, 3955–3958.
38 C. E. Hoyle and C. N. Bowman, Wiley Online LibraryCE Hoyle, CN Bowman, *Angew. Chem., Int. Ed.*, 2010, **49**, 1540–1573.
39 J. Camilleri, F. E. Montesin, K. Brady, R. Sweeney, R. V. Curtis and T. R. P. Ford, *Dent. Mater.*, 2005, **21**, 297–303.
40 C. T. W. Meereis, E. A. Münchow, W. L. de Oliveira da Rosa, A. F. da Silva and E. Piva, *J. Mech. Behav. Biomed. Mater.*, 2018, **82**, 268–281.
41 C. L. Davidson and A. J. Feilzer, *J. Dent.*, 1997, **25**, 435–440.
42 C. L. Davidson, A. J. de Gee and A. Feilzer, *J. Dent. Res.*, 1984, **63**, 1396–1399.
43 A. J. Feilzer, A. J. de Gee and C. L. Davidson, *J. Dent. Res.*, 1987, **66**, 1636–1639.
44 B. Van Meerbeek and J. De Munck, *Open Dent. J.*, 2003, **28**, 215–235.
45 F. Gonçalves, C. Pfeifer, J. Stansbury and S. Newman, *Dent. Mater.*, 2010, **26**, 697–703.
46 I. Sideridou, V. Tserki and G. Papanastasiou, *Biomaterials*, 2002, **23**, 1819–1829.
47 C. Floyd and S. Dickens, *Dent. Mater.*, 2006, **22**, 1143–1149.
48 J. L. Ferracane, *Dent. Mater.*, 2005, **21**, 36–42.
49 I. Sideridou, M. Karabela and E. Vouvoudi, *Dent. Mater.*, 2011, **27**, 598–607.
50 D. Lippert, J. Burnham and D. Seo, *Langmuir*, 2023, **39**, 5021–5030.
51 A. P. P. Fugolin and C. S. Pfeifer, *J. Dent. Res.*, 2017, **96**, 1085–1091.